Modeling liquid crystal bilayer structures with minimal surfaces

J. D. Enlow[a] and R. L. Enlow
Mathematics and Statistics Department, University of Otago, Dunedin, New Zealand

K. M. McGrath
Chemistry Department, University of Otago, Dunedin, New Zealand

M. W. Tate
Physics Department, Cornell University, Ithaca, New York 14853

(Received 18 August 2003; accepted 29 October 2003)

This paper describes a new convenient and accurate method of calculating x-ray diffraction integrated intensities from detailed cubic bilayer structures. The method is employed to investigate the structure of a particular surfactant system (didodecyldimethylammonium bromide in a solution of oil and heavy water), for which single-crystal experimental data have recently been collected. The diffracted peak intensities correlate well with theoretical structures based on mathematical minimal surfaces. Optimized electron density profiles of the bilayer are presented, providing new insight into key features of the bilayer structure. © *2004 American Institute of Physics.*
[DOI: 10.1063/1.1635811]

I. INTRODUCTION

The term ''liquid crystal'' is commonly associated with the simple polymer liquid crystal phase used in familiar liquid crystal displays, but the term also refers to structures with far greater complexity. Liquid crystals have a range of diverse roles in industry, for example in the formation of stable hydrocarbon foams, and in biological systems, as the structural bilayer forming cell membranes.[1] One particularly interesting class of structures that can be observed in appropriate solutions of surfactant, oil and water are called ''cubic bicontinuous liquid crystals.'' They have cubic unit cells and create two nonintersecting water labyrinths separated by the surfactant bilayer.

The connection between minimal surfaces (surfaces with minimal area for a given perimeter) and cubic bicontinuous surfactant liquid crystals has attracted much attention in the past decade. Analysis of curvature and bending frustration in the surfactant bilayers,[2–4] atomic simulations,[5] and phase models[6,7] indicate that minimal surfaces are strong candidates for these bilayer central surfaces. However, despite novel approaches to the complexities of modeling the intricate mesophases, conclusive evidence supporting minimal surface based structures has yet to be found.

Past research has compared x-ray diffraction data from large numbers of randomly orientated crystallites (''powder'' diffraction) with theoretical intensity calculations based on coarse approximations of the charge density throughout the liquid crystal.[8–12] This approach allows easy comparison with readily obtainable experimental data and greatly simplifies calculation of the theoretical intensities. However, it reveals little about the detailed atomic structure of the bilayer and it gives only an indication of whether or not a particular central surface is appropriate. On the other hand, x-ray diffraction data from a single large liquid crystal allow full space group determination, and theoretical models accounting for the major features of the bilayer molecular structure give a more informative comparison with the experimental intensity data. This paper introduces flexible and accurate methods of intensity calculation for both multiple and single crystal diffraction processes. These methods are used to investigate a particular surfactant system, and to add new evidence to the premise that surfactant liquid crystals can have structures whose shapes are based on minimal surfaces.

II. MINIMAL SURFACES

The liquid crystals under investigation are observed to have translational symmetry in three principal directions, so only triply periodic minimal surfaces (TPMS) are considered here. In 1856 the first example of a TPMS, the double diamond, was discovered and studied by Schwarz[13,14] (see Fig. 1). Schwarz also discovered the primitive, and a closely related surface known as the gyroid was discovered by Schoen.[15] These three surfaces differ only by a simple conformal mapping (Bonnet transformation). Schoen also discovered the I-WP surface, which has the same symmetry properties as Schwarz's primitive. Many minimal surfaces have since been discovered, and systematic methods of finding minimal surfaces have been developed.[16–21]

Minimal surfaces can be constructed exactly from Weierstraß parametrizations.[16,22,23] These parametrizations can be represented as the inverse of composite Gauss and stereographic projection mappings from a patch of the surface to the complex plane. Because the Gauss map is used, all points on the surface with parallel normal vectors map to the same point in the complex plane. The inverse mapping is thus unable to construct the entire surface, and is used only to produce a small fundamental patch of the surface. A complete unit cell can then be built using symmetry operations characterizing the surface (see Fig. 2). The inverse mapping

[a]Electronic mail: jenlow@maths.otago.ac.nz

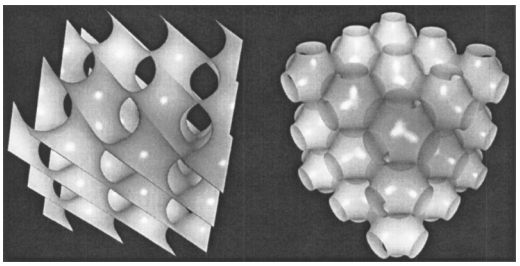

FIG. 1. Portions of Schwarz's double diamond (left) and primitive (right) triply periodic minimal surfaces.

is somewhat cumbersome, involving an integral with associated singularities at locally planar points on the surface, but has been evaluated analytically for several of the surfaces of interest.[24–27]

Determining suitable candidates for liquid crystal bilayer central surfaces begins with consideration of the symmetry properties of the liquid crystal, which places it in one of 230 possible space groups. The DDAB/oil/water system under investigation was found to form three bicontinuous cubic liquid crystal phases at different concentrations, with space groups $Ia\bar{3}d$, $Im\bar{3}m$, and $Pn\bar{3}m$ (consistent with previous analyses[10,28–31]). The second consideration is the energetic stability of the surface, which generally favors surfaces of low genus.[32] The expected bilayer thickness relative to the size of the unit cell also plays a role in limiting the genus of the central surface. Of the known TPMS in the space groups of interest here, the best candidates are the Primitive and I-WP ($Im\bar{3}m$ space group), the Double Diamond ($Pn\bar{3}m$ space group) and the Gyroid and S surface ($Ia\bar{3}d$ space group).[3,4,17]

III. NUMERICAL CALCULATION OF RELATIVE INTEGRATED INTENSITIES

In order to capture the full intensity contribution of the x-ray diffraction peaks, and to minimize the effects of experimental parameters, only the ''relative integrated intensities'' of the experimental and theoretical results are compared. The integrated intensity is the integral of the intensity over the detector screen region and the crystal rotations for which the intensity is significantly greater than background noise. These integrated intensity values are divided by the integrated intensity value for the first strong peak of the series to produce relative integrated intensities.

The integrated intensity at a peak identified by Bragg indices hkl is of the form[33]

$$I_{hkl} \propto \Upsilon_{hkl} |F_{hkl}|^2, \tag{1}$$

where Υ_{hkl} represents the product of various correction factors (such as the Lorentz and polarization factors), and the structure factor F_{hkl} is the Fourier transform of the electron density within a unit cell of the liquid crystal. This relationship can be used for large liquid crystals made up of nonuniform unit cells, becoming exact as the liquid crystal size tends toward infinity, provided that the electron density used in the Fourier transform is that of the *average* of all unit cells in the liquid crystal. For convenience we approximate the average electron density, which will include deviations in the unit cell contents as well as lattice imperfections, by a near-ideal electron density distribution convoluted with a three-

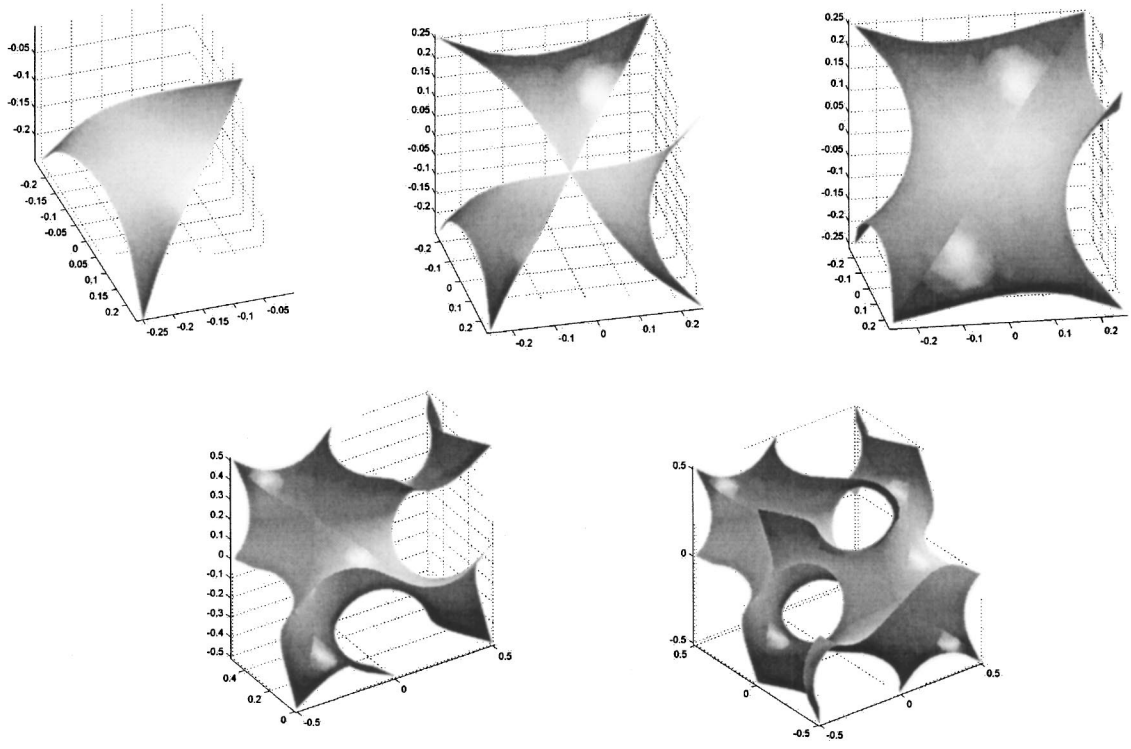

FIG. 2. Construction of a unit cell of the gyroid minimal surface from a fundamental patch (''Flackenstück'') using symmetry operations.

dimensional Gaussian. This Gaussian can be incorporated into Υ_{hkl}, and taking its standard deviation as σ, the necessary factor is $\Xi_{hkl}=\exp[-4\pi^2\sigma^2(h^2+k^2+l^2)]$. Note that this term is in the same form as the (relatively small[9]) Debye–Waller temperature factor, which can be absorbed by increasing σ by an appropriately small amount.

We generate the electron density distribution for an averaged unit cell by uniformly decorating the theoretical bilayer central surface with a given profile, which is chosen to reflect the important features of the bilayer composition. This decoration neglects any variation in the averaged bilayer thickness which is consistent from unit cell to unit cell. Even if such variation is present and significant in the experimental systems, it is probable that the existing experimental data lack enough information to determine the variations to any degree of accuracy (see Sec. V B).

The minimal surfaces that are used as the bilayer central surfaces are calculated from exact Weierstraß parametrizations[22,25–27] and stored as Delaunay triangulations. The spacing of the points across the surface is concentrated toward regions of high Gaussian curvature, allowing approximately 3000 triangles to accurately represent a unit cell. At any point in the unit cell the shortest distance to the surface is readily calculated from the triangulation, then the electron density is assigned from the profile accordingly.

Once the electron density distribution has been described in terms of some arbitrarily complex profile, the structure factor is calculated by taking the Fourier transform of this electron density distribution. To evaluate the Fourier transform we use an analogous approach to that outlined by Garstecki and Holyst,[11] but without their surface and curvature approximations. These approximations are necessary for their development, and the removal of the approximations requires a reformulation of the calculation procedure. We begin by transforming the unit cell into dimensionless coordinates (using the width of the cubic unit cell, commonly known as the lattice parameter, as the characteristic length). Then $d_{(x,y,z)}$, the shortest dimensionless distance from the point (x,y,z) in the unit cell to the central surface, is calculated, and an upper bound D is determined such that

$$\forall(x,y,z)\in[0,1]^3, \quad d_{(x,y,z)}<D.$$

The unit cell's volume is then divided into M bands, $B_1,\ldots,B_M$, with band B_i representing all points (x,y,z) such that $(i-1)D/M\leqslant d_{(x,y,z)}<i(D/M)$. The Fourier transform of the electron density can now be calculated as

$$F_{hkl}\approx\sum_{i=1}^{M} f_i\rho_i, \tag{2}$$

where ρ_i is the electron density at dimensionless distance $(i-\frac{1}{2})(D/M)$ from the central surface, and

$$f_i\equiv\int_{B_i} e^{2\pi i(h,k,l)\cdot\mathbf{r}}d^3\mathbf{r}. \tag{3}$$

These f_i values are bilayer-independent, and only need to be calculated and stored once for each central surface of interest. They can then be used for any desired electron density profile. In general however, the M sample points of the electron density profile will not adequately represent all of the profile features of interest. To compensate, we introduce a smoothed profile $f(\zeta)$ based on the band values f_i and the maximum distance-to-surface D, such that

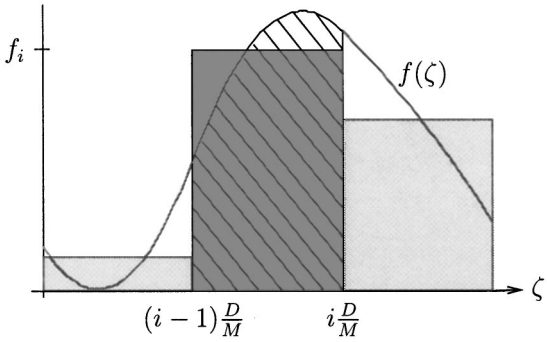

FIG. 3. Area-preserving quadratics are fitted to the f_i values.

$$F_{hkl}\approx\frac{M}{D}\int_0^D f(\zeta)\rho(\zeta)d\zeta. \tag{4}$$

This smoothing function must preserve the net contribution in each band, and satisfy $f(0)=f(D)=0$. A convenient interpolation scheme that is used here involves fitting a quadratic in each band, with the requirements that $f(\zeta)$ is smooth throughout $\zeta\in(0,D)$ and that area is preserved (see Fig. 3).

IV. COMPARISON WITH STRIP MODELS

Clerc and Dubois-Violette[8] developed a convenient approximation of the structure factor expression for "strip" models (constant electron density out to some distance L away from the surface and zero beyond, see Fig. 4). They use the exact Weierstraß method of surface generation, but their structure factor approximation represents constant electron density only for locally planar regions of the bilayer central surface, and fails when the radius of curvature is comparable to L.[11] They build the bilayer in a unit cell by decorating only the region of the central surface which lies within that unit cell, neglecting the contribution from parts of the bilayer which have the corresponding central surface patch in an adjacent unit cell (for example, portions of the bilayer that lie in the corners of the gyroid unit cell). Despite these shortcomings, their model is shown to correlate reasonably well with experimental results for a number of systems. They fit their data to the experimental results using two parameters, the step function half-width and the mean atomic displacement in the temperature factor. Their results, together with results from the methods of this work (when restricted to the

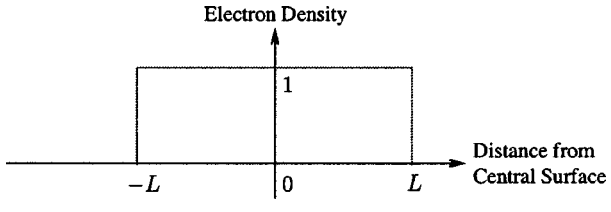

FIG. 4. Step function electron density profile.

TABLE I. Comparison of experimental and modeled relative integrated intensities from Ref. 8 with the models presented here (restricted to "strip" profiles matching those used by Clerc *et al.* and thus restricting the present model's ability to provide an optimal match to the experimental data). The starred data set represents a bilayer half-thickness of 0.125, a rough estimate by Clerc from geometrical considerations, rather than 0.098 in the unstarred data set (Clerc's fitted value). The + symbols represent small values ($\leqslant 2$).

	Lecithin				Galactolipid		
hkl	Experimental	Model (Ref. 8)	This work	This work*	Experimental	Model (Ref. 8)	This work
211	100	100	100	100	100	100	100
220	37	34	42	39	62	36	44
321	1	0	0	0	1	1	1
400	2	4	5	0	9	7	9
420	+	1	1	0	3	3	4
332	+	1	1	4	5	3	5
422	+	0	0	2	1	1	1
431	+	0	0	2	0	0	0
521	+	0	0	0	0	0	0
440	+	0	0	0	0	0	0
611	3	1	1	2	4	0	0
532	1	0	0	0	2	0	0
620	0	0	0	0	0	0	0

simple strip model profile), are shown in Table I, where in all cases the parameters optimized for their model are used. These parameter values are suboptimal for the more accurate methods used here.

Garstecki and Holyst extend Clerc's strip model by introducing a correction factor, independent of the bilayer width, in an attempt to reduce the errors associated with the structure factor approximation.[11,12] For convenience they no longer consider exact minimal surfaces, but rely on simple parametric approximating surfaces based on Fourier expansions.[17,34] They propose this variation of Clerc's method as a standard method of investigation, and suggest that it may be appropriate for modeling any electron density profile as a weighted combination of (approximately) uniform films, which is similar to the approach used in this work. They provide convenient tables of values for a collection of approximated surfaces, and demonstrate that their method produces good correlation with existing experimental data sets. With their correction factors, the nonuniformity of the approximated film which decorates the central surface introduces only minor errors for small film thicknesses, but still causes failure of the model further from the bilayer central surface. Figure 5 shows absolute intensities versus film half-thickness for two peaks of the gyroid minimal surface, illustrating the behavior of their approximations. While their method is clearly a useful tool for simple film decorations, the inherent approximating errors make it less likely to be a good choice for the sensitive process of detailed electron density profile determination.

Harper *et al.*[35,36] also generate Fourier amplitudes for

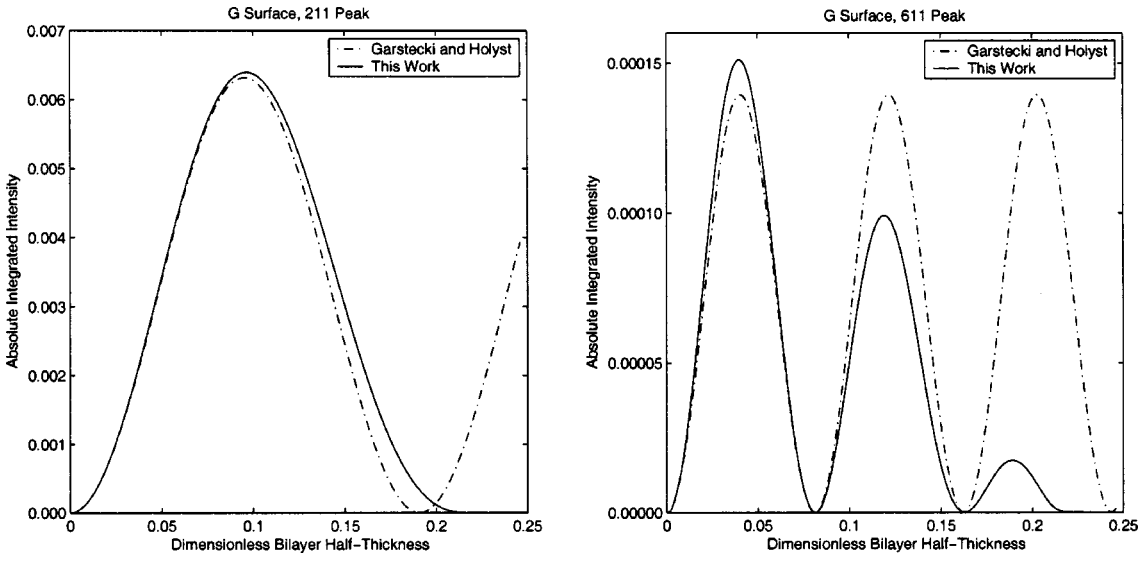

FIG. 5. Absolute integrated intensity vs film half-thickness for two peaks of the gyroid minimal surface. Approximation in the structure factor expression and bilayer construction causes inaccuracies with the method of Garstecki and Holyst, which become large as the film thickness increases. (Note that dimensionless half-thicknesses over 0.1 represent large volume fractions above 55%, thus most systems are fairly well modeled using Garstecki and Holyst's methods.)

TABLE II. Relative integrated intensity comparison for thin strips of constant electron density decorating the double diamond minimal surface. Results for three dimensionless film half-thicknesses are shown.

	Double diamond					
	$l=0.02$		$l=0.16$		$l=0.20$	
hkl	Harper	This work	Harper	This work	Harper	This work
110	97.9	97.8	100.0	100.0	100.0	100.0
111	100.0	100.0	76.3	76.4	62.1	62.2
200	28.8	29.0	9.8	9.8	3.1	3.1
211	19.1	18.7	3.0	2.9	0.1	0.1
220	27.1	27.4	0.8	0.7	1.0	1.0
221	32.2	32.2	0.2	0.2	2.4	2.4
310	14.5	14.6	0.0	0.0	1.1	1.1
311	3.9	4.0	0.0	0.0	0.3	0.3
222	34.0	34.3	0.7	0.6	6.0	5.9
321	3.7	3.6	0.2	0.2	0.6	0.6
400	8.2	7.9	0.5	0.5	0.7	0.7
322	13.7	13.5	1.3	1.3	1.7	1.6

step function electron density profiles decorating minimal surfaces, but use a more accurate and computationally involved method than Clerc *et al.* Exact (Weierstraß) equations are used to generate patches of the minimal surface, which are then accurately approximated using parametric equations. The surfaces are triangulated, allowing for convenient calculation of surface integrals. The Fourier amplitudes of the bare minimal surface are compared to results from several other methods, with excellent agreement. Fourier amplitudes of strip models are evaluated by transforming the volume integral in the structure factor to a surface integral via the Abbè transformation. Harper's method is theoretically equivalent to the method presented in this paper when restricted to strip profiles. However, due to their computationally different approaches, a comparison of the respective results provides a good check that the small approximations in both methods have negligible adverse effects. In Table II, integrated intensities based on Harper's Fourier amplitudes are compared to the results of this work for thin strip decorations of the double diamond minimal surface. A similarly close match is found for decorations of the primitive and gyroid surfaces. While the two methods of relative integrated intensity computation produce essentially the same results for step-function profiles, the method presented here is not limited to this simple case, but allows convenient integrated intensity calculation for *any* profile. This allows a more detailed analysis of the bilayer structure, and correspondingly better agreement between modeled and experimental relative integrated intensities.

V. SINGLE LIQUID CRYSTAL COMPARISON

Accurate experimental integrated intensity measurements are required in order to develop more detailed electron density profiles. Experimental single crystal data recently obtained by McGrath and Tate[37] provide a good foundation for investigation, and include integrated intensity measurements for liquid crystal phases with space groups $Pn\bar{3}m$, $Im\bar{3}m$, and $Ia\bar{3}d$ (those of the double diamond, primitive and gyroid minimal surfaces, respectively). Empirically determined parameters from the single crystal experimental samples are shown in Table III. The surfactant used is didodecyldimethylammonium bromide (DDAB), in a solution of heavy water (D_2O) and dodecane. The liquid crystalline domains are large (of the order of 1 mm), and exhibit small mosaic spreads of 0.7° ($Ia\bar{3}d$) to 3° ($Im\bar{3}m$).

TABLE III. Experimental parameters for the DDAB/$C_{12}H_{26}$/D_2O system.

	$Pn\bar{3}m$	$Im\bar{3}m$	$Ia\bar{3}d$
Lattice parameter (nm)	12.793	16.459	31.335
DDAB (wt %)	31.37	30.25	20.92
Dodecane (wt %)	5.49	6.30	2.88
D_2O (wt %)	63.14	63.45	76.20

While precise empirical determination of the electron density profile is not possible, a few simple assumptions allow estimation of the tail-chain length, the bilayer thickness and the volume fractions. Assuming that the disassociated bromide ions contribute little to the bulk charge, the average electron density of the water region is approximately $333e\ \mathrm{nm}^{-3}$. That of the hydrocarbon tail region is approximately $300e\ \mathrm{nm}^{-3}$.[35] The electron density in the head group region is unknown, but assuming a head group volume (including the nitrogen atoms and the methyl groups) of 0.2 times the tail-chain volume permits calculation of the parameters given in Table IV from the compositions by weight % in Table III. These approximate values are in reasonable agreement with those for similar systems[12,30,38] and give a starting point for the determination of the electron density profile.

A. Step-function profiles

If the primary electron density contrast is assumed to be between the water and hydrocarbon regions then the electron density profile may be modeled, as a first approximation,[11,12] by a simple step function profile. When combined with a large value of σ in Ξ_{hkl}, or equivalently a large temperature factor (as used in Ref. 8), the nonphysically sharp electron density contrast is smoothed, giving a gentle transition and allowing a better match to experimental data. Results for step-function profiles are given in Tables V and VI, with L taken to be the bilayer half-thickness values shown in Table IV. The dimensionless Gaussian standard deviation σ has been chosen to best fit the experimental results, and when multiplied by the characteristic unit cell length, the optimal values fall between 1.2 and 1.5 nm, indicating significant

TABLE IV. Parameters derived from the compositions by weight given in Table III. Volumes are given per unit cell.

Quantity	Units	Double diamond	Primitive	Gyroid
Tail volume	nm^3	712	1512	6858
Head group volume	nm^3	142	302	1372
Bilayer volume fraction		0.408	0.407	0.267
Hydrocarbon tail length	nm	1.14	1.20	1.10
Bilayer half-thickness	nm	1.39	1.45	1.34

TABLE V. Primary results, single crystal experimental relative integrated intensities compared to modeled values. The experimental values include the Lorentz correction factor, and the theoretical values naturally account for the Debye–Waller factor in their Gaussian distributions. The parameter σ has been fitted to the experimental data. The error measure is the sum of the squares of the differences in relative integrated intensities. The ''Full profile'' results are described in Sec. V B.

	Double diamond			Primitive			Gyroid		
hkl	Experimental	Step function	Full profile	Experimental	Step function	Full profile	Experimental	Step function	Full profile
110	100.0	100.0	100.0	100.0	100.0	100.0			
111	51.4	52.2	51.4						
200	8.6	6.4	9.1	79.7	84.0	80.5			
211	3.4	1.1	2.3	35.0	29.7	34.8	100.0	100.0	100.0
220	1.7	0.4	1.8	0.3	0.1	0.4	51.4	40.1	50.1
221	1.4	0.2	1.4						
310	0.1	0.0	0.6	0.9	0.4	0.5			
311	0.0	0.0	0.1						
222	0.4	0.0	0.5	5.7	3.4	5.7			
321	0.0	0.0	0.0	1.3	0.5	0.9	0.3	0.7	0.0
400	0.0	0.0	0.0	2.4	0.3	0.7	4.5	10.4	6.5
322	0.1	0.0	0.0						
411				0.5	0.1	0.4			
330				0.1	0.1	0.3			
420				0.0	0.0	0.1	3.4	6.0	2.3
332				0.3	0.0	0.1	7.4	8.4	7.5
422				0.1	0.0	0.0	3.2	2.6	1.9
431				0.0	0.0	0.0	2.5	1.1	1.4
521				0.0	0.0	0.0	0.0	0.1	0.4
440				0.0	0.0	0.0	2.0	0.0	0.1
σ		0.118	0.134		0.071	0.104		0.045	0.076
Error		14	2		58	4		177	14

disorder in the experimental liquid crystal. The value for the $Ia\bar{3}d$ (gyroid) phase is consistent with the values observed for step-function profiles in Ref. 8 for other gyroid-based systems ($0.02 \leqslant \sigma \leqslant 0.06$).

We eliminate the unbalanced I-WP and the high-genus S minimal surfaces as candidates for the bilayer central surfaces based on the results shown in Table VI. In particular the 211 peak of the $Im\bar{3}m$ experimental results is poorly modeled by the I-WP surface, and the S surface gives consistently low correlation with $Ia\bar{3}d$ experimental figures. Using detailed electron density profiles does not improve the results significantly for these surfaces.

TABLE VI. Single crystal relative integrated intensity comparison for I-WP and S minimal surfaces, based on a step function electron density profile.

hkl	Experimental $Im\bar{3}m$	I-WP *Surface*	*hkl*	Experimental $Ia\bar{3}d$	S Surface
110	100.0	100.0	211	100.0	100.0
200	79.7	80.5	220	51.4	15.2
211	35.0	2.2	321	0.3	7.2
220	0.3	2.8	400	4.5	11.0
310	0.9	4.8	420	3.4	0.1
222	5.7	0.8	332	7.4	0.1
321	1.3	0.0	422	3.2	0.0
400	2.4	0.1	431	2.5	0.0
σ		0.111	σ		0.131
Error		1129	Error		1481

B. Detailed electron density profiles

Construction of a more detailed electron density profile (that provides a better match to the experimental relative integrated intensities) allows further insight into the surfactant bilayer structure. The major scattering features of the DDAB/oil/water system are located at the bilayer central surface and within and near the head group region. A decrease in the electron density near the bilayer central surface is expected because of the higher probability of finding low-density hydrocarbon terminal methyl groups in the vicinity. The oil will reduce this effect to some extent, so it is unlikely that this will be the primary scattering feature that it is in other systems.[35,36] The scattering features of the outer portions of the bilayer will be determined by the relatively well-ordered head group atoms and their associated bromide counter-ions, both of which tend to increase the electron density (above that of the bulk water regions), and the methyl units attached to the head groups, which tend to reduce the electron density. It is not clear in advance whether the net effect will be best modeled by a single peak in the electron density, or by two or three closely spaced peaks in the vicinity of the head group location.

The calculation methods described in Sec. III allow complete freedom in choosing a model for the electron density profile, and we are limited in refining that model only by the experimental data (in particular the accuracy of the data and the number of significant peaks) together with our ability to optimize the parameters in the model. In this optimization,

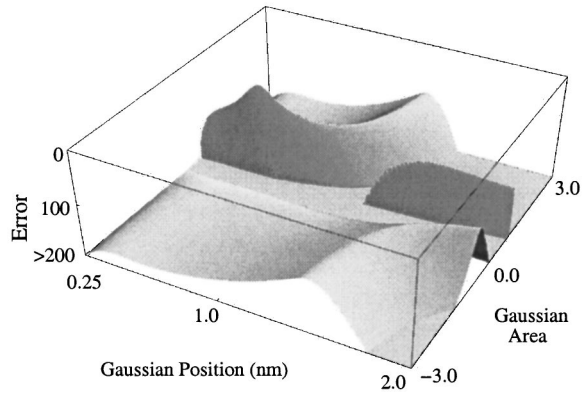

FIG. 6. Errors associated with parameter variation in the three Gaussian model using the gyroid minimal surface. The parameters represent the position of the head group Gaussian (nm from the central surface) and the area under the Gaussian (in e nm^{-1}).

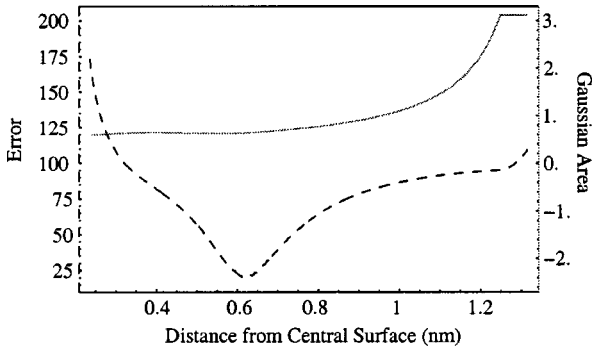

FIG. 7. Effects of varying the head group Gaussian position for the three Gaussian model using the gyroid minimal surface. This graph shows both the minimum error (dashed line) and the optimal Gaussian area (solid line) for a range of positions of this Gaussian.

the scalar objective function is taken to be the sum of the squares of the differences in relative integrated intensities between experimental data and theoretical models. Due to the complex interactions in the diffraction process, variations in the model parameters produce changes in this objective function that are generally not easy to predict. Finding optimal values for models with more than two or three parameters can be difficult. The parameter space in such models generally produces objective function values with awkward features, such as multiple local minima, small regions of low error that are difficult to find, and regions of instability (large variations for small changes in the parameters). This limits the usefulness of automated optimization techniques such as the downhill simplex method and the conjugate gradient method. If we restrict ourselves to models with only a few degrees of freedom, then we are able to determine the value of the objective function throughout our parameter space, giving a full description of the error (including the location of the global minimum). With this in mind we seek the model with the lowest number of parameters that gives a good fit to the experimental data in all three cases.

1. Three Gaussian model

The first improvement on the simple step function model consists of three Gaussians, one representing the lowered electron density in the tail region, and the other two representing the head group contributions (with one on each side of the bilayer). The relative integrated intensity results are invariant under linear transformations of the electron density (and hence the electron density profile), so we arbitrarily fix the size of the tail Gaussian without loss of generality. We then assign parameters to the size and position of the head group Gaussian. The resulting errors are graphed in Fig. 6 for the gyroid minimal surface. The best fit is obtained when the head group Gaussian is positioned well within the tail region, giving an error of 20. This Gaussian position is however inconsistent with the chemical composition of the bilayer. Experimental error and model limitations play key roles in determining this optimal position, so, rather than focusing solely on the best fit, we will instead look at the regions where the fit is good and the bilayer parameters lie within expected ranges. Figure 7 shows the effects of varying the Gaussian position on the minimal error and on the corresponding optimal Gaussian area. Relatively good fits are obtained (error$<$100) for Gaussian positions from 0.32 nm through to 1.25 nm. In all cases this Gaussian contributes a small local increase in the electron density, which we attribute to the relatively well-ordered nitrogen molecules in the surfactant head group region. We thus expect the location of these Gaussians to be approximately equal to the length of the hydrocarbon tail chain, which is estimated to lie in the range 1.0–1.3 nm for DDAB systems.[28,38,39] The experimental liquid crystals under consideration have only a small amount of oil added, so we would expect better fits towards the lower end of this range.

For the double diamond and primitive based structures, the graphs corresponding to Fig. 6 show large regions of nearly optimal parameter values. Considerably less information can be obtained in these cases, consistent with their nearly featureless experimental intensity distributions (see Table V). Fixing the head group Gaussian position at 1.0 nm (based on the gyroid analysis) results in the optimal profiles shown in Fig. 8. The area of the head group Gaussians in the gyroid profile is significantly different than that of the primitive and double diamond profiles, and the associated error in the case of the gyroid is relatively large (87 versus 10 for the primitive and 8 for the double diamond). This implies that the model is too simplistic to fit the experimental data well, motivating the inclusion of extra Gaussian distributions.

2. Five Gaussian model

We find that a five Gaussian model provides considerably improved correlation with the experimental intensity data. In this model one Gaussian is centered on the bilayer central surface and the other four are fixed in position in the vicinity of the head group region (two on each side of the bilayer). The widths of the Gaussians are approximated empirically, and the results are not particularly sensitive to the values chosen. As before we fix the area of the central Gaussian without loss of generality, leaving two parameters to be fitted (the areas of the remaining two Gaussians). A unique minimum is present for all three phases of liquid crystal con-

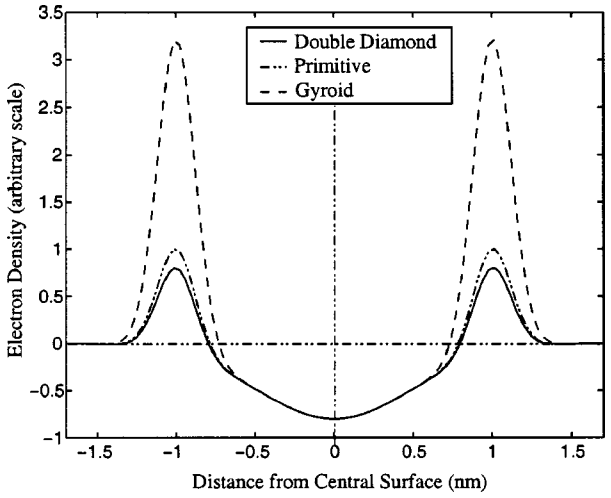

FIG. 8. Electron density profiles for the three Gaussian model, with the head group Gaussians fixed at 1.0 nm from the bilayer central surface. Relative integrated intensity is invariant under linear transformations of the electron density, so the vertical axis scaling is arbitrary.

sidered, with the corresponding electron density profiles being very similar (see Fig. 9). The resulting relative integrated intensities are tabulated in the ''full profile'' columns of Table V.

The minor differences between these three optimal profiles are likely to be a result of surfactant and oil concentration and the central surface properties. Other factors may significantly contribute to these differences, including experimental error and temperature effects. We attribute the positive Gaussian to the relatively well-ordered head group atoms, and the negative Gaussian to the outer methyl groups attached to the nitrogen atoms in the head groups. The magnitude of these Gaussians, relative to that of the central negative Gaussian (which represents on average a $33e\ \mathrm{nm}^{-2}$ reduction from the electron density of bulk water), are considerably larger than expected. In addition, given the flexibility of multiple parameter models, the particular profile model that was chosen is unlikely to be unique in providing a close match to the experimental data. It would be informative to compare the profiles of Fig. 9 with those for lamellar or micellar phases of the ternary mixture, especially to determine whether the large head group Gaussians are a true feature of the DDAB bilayers. However, all three phases produce similar optimal profiles with this model, the match is simultaneously excellent for all three surfaces, and the profiles represent a simple bilayer configuration based on empirical data. These points indicate that the profiles should represent the gross features well. Most important, the consistently high correlation between experimental and theoretical results adds significant weight to the premise that surfactant liquid crystals can form structures whose shapes are based on mathematical minimal surfaces.

Clearly the use of a full profile rather than a simple film decoration allows a better match to the experimental data. The methods of Sec. III provide a sound framework for detailed studies involving complex profiles. In addition, the approximated structure factor equation developed by Garstecki and Holyst [Eq. (24) in Ref. 11] provides a direct and simple method of obtaining a near-optimal profile, which could then be checked and refined (if necessary) using the methods presented here. With these methods, using a detailed electron density profile is no longer a difficult and computationally intensive task, and good control of numerical and modeling errors can be maintained.

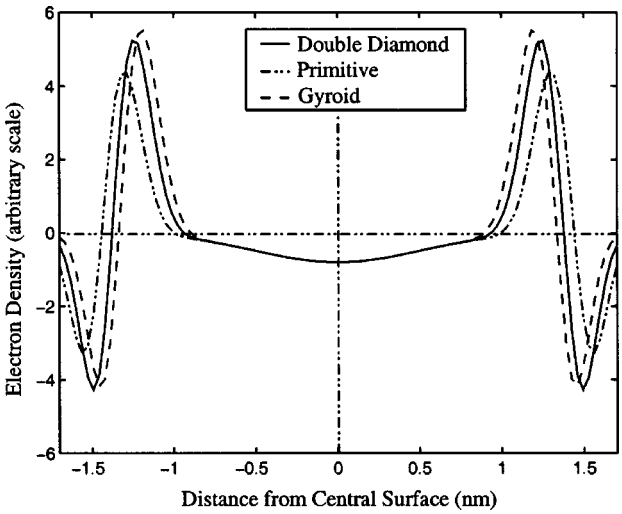

FIG. 9. Fitted DDAB electron density profiles for the five Gaussian model. Relative integrated intensity is invariant under linear transformations of the electron density, so the vertical axis scaling is arbitrary. The corresponding peak intensities are shown in Table V.

VI. CONCLUDING REMARKS

In this paper we give an accurate and computationally efficient method of relative integrated intensity calculation for bilayers centered on triply periodic surfaces. The method described is limited to a fixed electron density profile decorating the central surface in the averaged unit cell of the liquid crystal, but places no restrictions on that profile. It provides the accuracy benefits of using true minimal surfaces, and makes no curvature approximations. We demonstrate that the method produces results consistent with published data, and improves on the results in Refs. 8 and 11. Using this method we fit Gaussian-based electron density profiles to x-ray diffraction data from single crystal experimental samples of a DDAB/oil/water surfactant system. We find very high correlation of relative integrated intensity values between samples of the $Ia\bar{3}d$, $Im\bar{3}m$, and $Pn\bar{3}m$ phases and the corresponding theoretical models. We find that the primitive, double diamond and gyroid minimal surfaces are consistent with the experimental data, and we eliminate the S and I-WP minimal surfaces as candidates for these liquid crystal phases. This analysis provides further evidence in support of the premise that minimal surfaces are a fundamental feature of bicontinuous cubic liquid crystalline structures. The methods described provide a sound framework for detailed investigation of small angle x-ray diffraction data obtained for other cubic systems.

[1] S. Hyde, S. Andersson, K. Larsson, Z. Blum, T. Landh, S. Lidin, and B. W. Ninham, *The Language of Shape* (Elesvier Science, Amsterdam, 1997).
[2] J. Charvolin and J. F. Sadoc, Proc. R. Soc. London, Ser. A **354**, 2173 (1996).
[3] S. T. Hyde, Colloq. Phys. **C7**, 51 (1990).
[4] U. S. Schwarz and G. Gompper, Langmuir **17**, 2084 (2001).
[5] S.-J. Marrink and D. P. Tieleman, J. Am. Chem. Soc. **123**, 12383 (2001).
[6] A. Ciach and R. Holyst, J. Chem. Phys. **110**, 3207 (1999).
[7] W. T. Gozdz and R. Holyst, Phys. Rev. E **54**, 5012 (1996).
[8] M. Clerc and E. Dubois-Violette, J. Phys. II **4**, 275 (1994).
[9] P. Garstecki and R. Holyst, J. Chem. Phys. **113**, 3772 (2000).
[10] P. Garstecki and R. Holyst, J. Chem. Phys. **115**, 1095 (2001).
[11] P. Garstecki and R. Holyst, Langmuir **18**, 2519 (2002).
[12] P. Garstecki and R. Holyst, Langmuir **18**, 2529 (2002).
[13] H. Schwarz, Monatsber, Berlin Akad. **3**, 149 (1865).
[14] H. Schwarz, *Gesammelte Mathematische Abhandlungen* (Springer, Berlin, 1890).
[15] A. H. Schoen, Technical Report No. TN D-5541, NASA, Washington D.C., 1970.
[16] A. Fogden, Colloq. Phys. **C7**, 51 (1990).
[17] U. Schwarz and G. Gompper, Phys. Rev. E **59**, 5528 (1999).
[18] H. Karcher and K. Polthier, Philos. Trans. R. Soc. London, Ser. A **354**, 2077 (1996).
[19] K. A. Brakke, Philos. Trans. R. Soc. London, Ser. A **354**, 2143 (1996).
[20] A. Fogden and S. T. Hyde, Acta Crystallogr., Sect. A: Found. Crystallogr. **48**, 442 (1992).
[21] A. Fogden, J. Phys. I **2**, 233 (1992).
[22] K. Weierstraß, Monatsber. Berliner Akad. **3**, 612 (1866).
[23] H. Terrones, Colloq. Phys. **C7**, 51 (1990).
[24] D. Cvijovic and J. Klinowski, Chem. Phys. Lett. **226**, 93 (1994).
[25] P. J. F. Gandy, D. Cvijovic, A. L. Mackay, and J. Klinowski, Chem. Phys. Lett. **314**, 543 (1999).
[26] P. J. F. Gandy and J. Klinowski, Chem. Phys. Lett. **321**, 363 (2000).
[27] P. J. F. Gandy and J. Klinowski, Chem. Phys. Lett. **322**, 579 (2000).
[28] P. Barois, S. Hyde, B. Ninham, and T. Dowling, Langmuir **6**, 1136 (1990).
[29] S. Radiman, C. Toprakcioglu, L. Dai, and A. R. Faruqi, Colloq. Phys. **C7**, 51 (1990).
[30] P. J. Maddaford and C. Toprakcioglu, Langmuir **9**, 2868 (1993).
[31] A. Linhananta and D. E. Sullivan, Phys. Rev. E **57**, 4547 (1998).
[32] S. T. Hyde, J. Phys. Chem. **93**, 1458 (1989).
[33] *International Tables for X-Ray Crystallography*, edited by J. S. Kasper and K. Lonsdale (International Union of Crystallography, 1967), Vol. II.
[34] A. L. Mackay, Philos. Trans. R. Soc. London, Ser. A **442**, 47 (1993).
[35] P. E. Harper and S. M. Gruner, Eur. Phys. J. E **2**, 217 (2000).
[36] P. E. Harper, S. M. Gruner, R. N. A. H. Lewis, and R. N. McElhaney, Eur. Phys. J. E **2**, 229 (2000).
[37] K. McGrath and M. Tate (private communication).
[38] S. T. Hyde, Colloids Surf., A **103**, 227 (1995).
[39] P. Barois, D. Eidam, and S. T. Hyde, Colloq. Phys. **C7**, 51 (1990).